THE JOURNAL OF PHYSICAL CHEMISTRY LETTERS
A JOURNAL OF THE AMERICAN CHEMICAL SOCIETY

pubs.acs.org/JPCL

Letter

Simultaneous Localization of Two High Affinity Divalent Metal Ion Binding Sites in the Tetracycline RNA Aptamer with Mn^{2+}-Based Pulsed Dipolar EPR Spectroscopy

Thilo Hetzke, Marc Vogel, Anna-Lena Johanna Halbritter, Subham Saha, Beatrix Suess, Snorri Th. Sigurdsson, and Thomas F. Prisner*

Cite This: *J. Phys. Chem. Lett.* 2023, 14, 11421−11428

Read Online

ACCESS | Metrics & More | Article Recommendations | Supporting Information

ABSTRACT: Mg^{2+} ions play an essential part in stabilizing the tertiary structure of nucleic acids. While the importance of these ions is well documented, their localization and elucidation of their role in the structure and dynamics of nucleic acids are often challenging. In this work, pulsed electron−electron double resonance spectroscopy (PELDOR, also known as DEER) was used to localize two high affinity divalent metal ion binding sites in the tetracycline RNA aptamer with high accuracy. For this purpose, the aptamer was labeled at different positions with a semirigid nitroxide spin label and diamagnetic Mg^{2+} was replaced with paramagnetic Mn^{2+}, which did not alter the folding process or ligand binding. Out of the several divalent metal ion binding sites that are known from the crystal structure, two binding sites with high affinity were detected: one that is located at the ligand binding center and another at the J1/2 junction of the RNA.

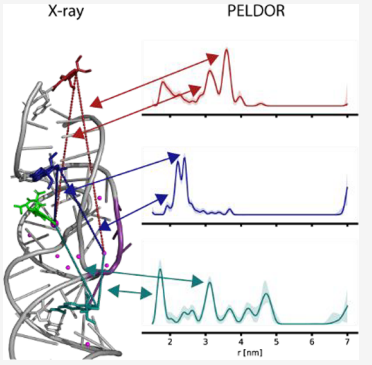

Metal cations are essential for stabilizing nucleic acids and ensuring proper folding of their tertiary structure, in particular, K^+ and Mg^{2+} ions. Generally speaking, monovalent cations like Na^+ or K^+ are "diffuse" cations, which do not form specific and close-range interactions with the negatively charged backbone of the nucleic acid molecule. Instead, these ions form electrostatic long-range interactions with the molecule of interest.[1,2] Divalent cations, in particular Mg^{2+}, also participate in such electrostatic interactions but additionally are important in stabilizing nucleic acid structural motifs by direct coordination. Techniques to sample the diffuse or direct interaction of Mg^{2+} to the nucleic acid include, among other methods, nuclear magnetic resonance (NMR) spectroscopy,[3] fluorescence resonance energy transfer (FRET) measurements,[4] small-angle X-ray scattering (SAXS),[5] X-ray crystallography,[6] and molecular dynamics (MD) simulations.[7] Localization of directly coordinated Mg^{2+} ions, and metal ions in general, is a nontrivial task that can lead to experimental difficulties. For example, NMR can sample the metal ion only indirectly, e.g., via ^{31}P NMR, paramagnetic relaxation enhancement (PRE), or pseudocontact shifts (PCS). In addition, liquid-state NMR is limited by the size of the nucleic acid due to line width broadening that originates from an increased rotational correlation time.[8] Seeding of single crystals for X-ray crystallography can be a challenging endeavor. Furthermore, assignment and verification of the Mg^{2+} ion binding sites can be difficult with X-ray crystallography, and examples of erroneous assignments can be found in the literature.[6] Recently, a machine-learning approach was proposed to predict Mg^{2+} binding sites in RNA.[9]

Pulsed dipolar spectroscopy (PDS) describes several techniques within electron paramagnetic resonance (EPR) spectroscopy to probe the dipolar coupling of two or more paramagnetic spin systems of a macromolecule. Because the dipolar coupling is inversely proportional to r^3, PDS can be used to obtain the distance r between paramagnetic spin centers. Nitroxide probes are frequently used because they are stable radicals with spin-Hamiltonian parameters and relaxation properties that are well suited for detection with PDS techniques.[10−16] Paramagnetic metal ions like Fe^{3+}, Mn^{2+}, Co^{2+}, Ni^{3+}, Cu^{2+}, and Gd^{3+} can be used for PDS as well,[17−19] and some of these ions exist as naturally occurring cofactors in enzymes. Another possibility to make a biopolymer EPR-active is to substitute diamagnetic Mg^{2+} with paramagnetic Mn^{2+}.[20,21]

Here we describe the application of a PDS technique called pulsed electron−electron double resonance (PELDOR) spectroscopy[22,23] (also called DEER) to localize high-affinity Mg^{2+} binding sites and to assess their relative affinities in nucleic acids. Measurements were performed on a 50 nucleotide long

Received: September 12, 2023
Revised: December 5, 2023
Accepted: December 5, 2023
Published: December 12, 2023

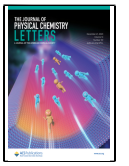

https://doi.org/10.1021/acs.jpclett.3c02566
J. Phys. Chem. Lett. 2023, 14, 11421−11428

tetracycline (TC) RNA aptamer that binds the antibiotic TC with an exceptionally high affinity (K_d = 770 pM at 10 mM Mg^{2+}) and is widely used as a synthetic riboswitch.[24−30] It is known that the aptamer binds its ligand TC via a Mg^{2+} ion. Additional Mg^{2+} ions are known to interact with the aptamer to ensure its folding to a stable tertiary structure.[31−36] Although the crystal structure sheds light on the additional Mg^{2+} binding positions,[37] little is known about the affinity of these sites and their relevance for folding of the aptamer. To enable PELDOR measurements, diamagnetic Mg^{2+} was substituted with paramagnetic Mn^{2+}, shown by isothermal titration calorimetry not to affect ligand binding,[32] and using different singly labeled nitroxide TC aptamer mutants. PELDOR experiments on the different mutants were then performed at different Mn^{2+} concentrations to probe the nitroxide−Mn^{2+} dipolar coupling. The experimental PELDOR distances were compared to theoretical distances derived from the crystal structure,[37] revealing localization of two high-affinity sites. A trilateration proof-of-concept study using EPR has been shown for a Cu^{2+} azurin protein.[38]

Figure 1A shows the secondary structure of the three spin labeled TC aptamer constructs. Positions C3 and C15 have

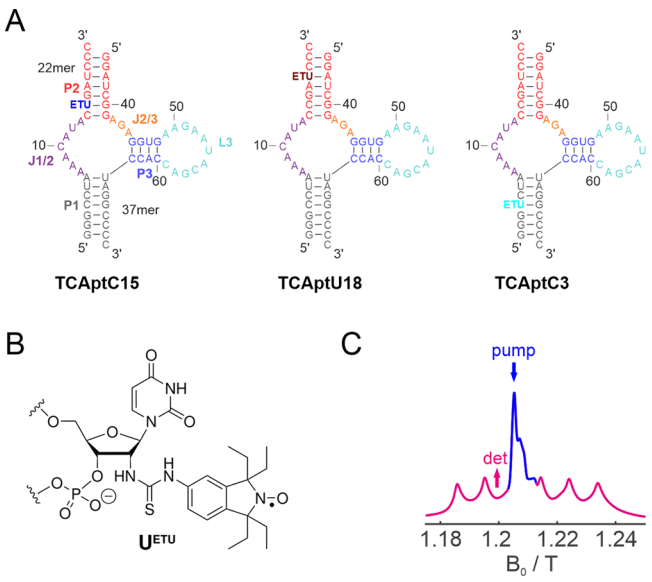

Figure 1. (A) Secondary structure of the TC aptamer used in this study. The three different labeling positions for the ETU spin label are indicated (left: TCaptC15; middle: TCaptU18; right: TCaptC3). Residue numbers are based on the secondary structure of the wild-type construct.[25,30] (B) Chemical structure of the tetraethylisoindoline nitroxide spin label (ETU spin label). The spin label is attached after solid-phase synthesis to a 2′-amino-modified oligonucleotide. (C) EPR spectrum of a singly ETU labeled TC aptamer with 0.22 mM Mn^{2+} in the presence of 0.165 mM TC. Magenta: EPR signal of Mn^{2+}; blue: EPR signal of the nitroxide. The nitroxide spectrum obscures a hyperfine peak of the central Mn^{2+} transition.

recently been used for spin labeling in a previous nitroxide−nitroxide PELDOR study.[31] Figure 1B shows the structure of the semirigid ETU spin label, previously shown to exhibit a low degree of internal freedom, yielding rather narrow distance distributions.[15,39] Covalent labeling of ETU was achieved by postsynthetic labeling of a 2′-amino nucleotide,[15] and more information can be found in Section 1 of the Supporting Information. Native PAGE analysis and fluorescence titration spectroscopy measurements did not indicate any perturbation by the spin labels (Figures S1 and S2). All constructs contained a C-overhang to prevent helical end-to-end stacking.[40]

To compare the PELDOR distance distributions to crystal structure distances, a molecular modeling approach with an optimized spin label structure was used. This approach was successfully used in a previous study,[39] and more information can be found in Section 6 of the Supporting Information. The sequence of the constructs used in this publication and of the crystal structure differs slightly at the ends of helical stems P1 and P2. In these regions, the crystal structure shows a rather unperturbed dsRNA with no resolved divalent metal ion binding sites, and it was shown in previous studies that changes and loop deletions in these regions do not affect the function and structure of the aptamer.[30,31] The U−A base pair in stem P2 that contains the ETU spin label (Figure 1A, TCAptU18) is a C−G base pair in the crystal structure (Figure S9). In the modeling approach, the ETU spin label was consequently connected to the 2′-N atom of a cytidine.

The final structure obtained with PyMOL is shown in Figure 2. TC is shown green, and the three different labeling positions are shown in blue (C15), dark red (U18), and turquoise (C3). The Mg^{2+} ions identified in the crystal structure are shown in magenta. The AAAA-motif (A6, A7, A8, and A9) in the J1/2 junction is highlighted purple. In this region, the backbone makes a U-turn. This rather uncommon structural motif is stabilized by a Mg^{2+} ion that is directly coordinated by two oxygen atoms of the phosphate backbone. In the crystal structure of the TC aptamer, no other Mg^{2+} ions are directly coordinated by two or more oxygen atoms from the phosphate backbone. This suggests tight binding and high affinity for the AAAA-Mg^{2+} ion. The expected crystal structure distances from the nitroxides to the Mg^{2+} ion in the TC-binding pocket (called TC-Mg^{2+} hereafter) and the Mg^{2+} ion at the AAAA-motif (called AAAA-Mg^{2+} hereafter) ranged from 1.79 to 3.62 nm (Figure 2). Accessible distances for PELDOR lie in the range 1.8−10 nm; therefore, the expected distances in the current study are ideally suited for an investigation with PELDOR.[41]

To localize and investigate the relative affinity of divalent metal ion binding sites in the TC aptamer, nitroxide-Mn^{2+} PELDOR measurements were performed at Mn^{2+} concentrations of 0.22 and 0.45 mM. A previous study showed a significant change of flexibility of the tertiary structure upon adding TC at these concentrations.[31] At higher divalent ion concentrations of 3 mM, the flexibility of the tertiary structure did not change upon addition of TC. Thus, the tertiary structure seems to be already stabilized at these high concentrations, even in the absence of TC. Measurements in the presence and absence of TC were only performed at 0.45 mM Mn^{2+} because of the limited sample amount of spin labeled RNA; measurements at 0.22 mM Mn^{2+} were only performed in the presence of TC.

Figure 1C shows an EPR spectrum of TCaptC15 with 0.45 mM Mn^{2+} in the presence of TC. The spectrum is dominated by the 6-line pattern of the Mn^{2+} electron spin (S = 5/2) that arises due to strong hyperfine coupling to the ^{55}Mn hyperfine nucleus (I = 5/2, 100% natural abundance). The third hyperfine line from the left is obscured by the EPR spectrum of the nitroxide (S = 1/2). The nitroxide spectrum results from the **g**-tensor anisotropy and the hyperfine coupling anisotropy to the ^{14}N nucleus (I = 1). The aforementioned interactions and the EPR line width are too large to resolve the dipolar interactions between Mn^{2+} and the nitroxide. For all PELDOR

https://doi.org/10.1021/acs.jpclett.3c02566
J. Phys. Chem. Lett. 2023, 14, 11421−11428

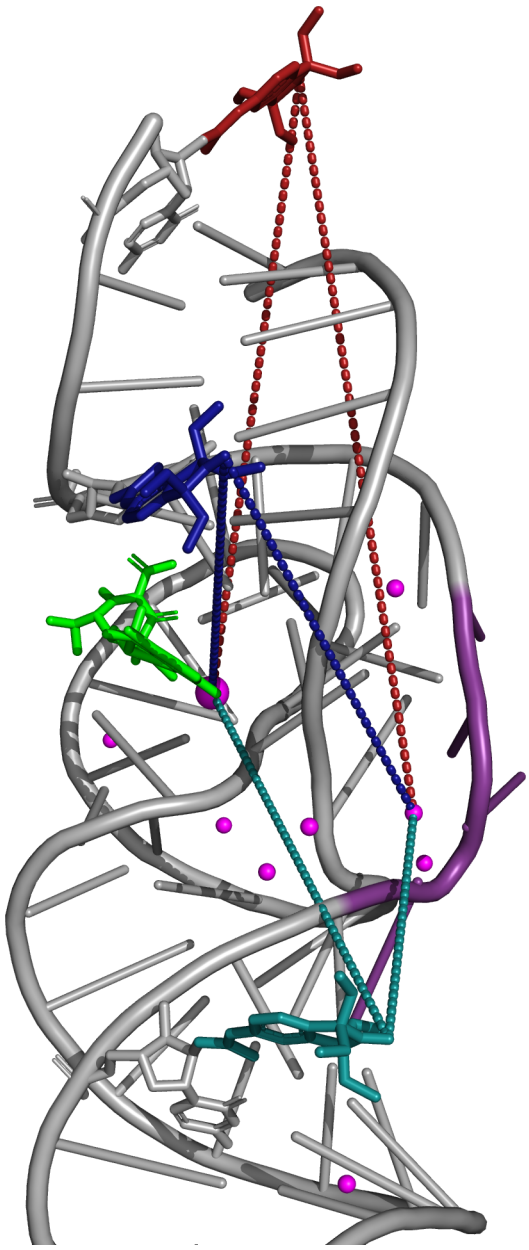

Figure 2. Expected tertiary structure of the constructs used in the present study, based on crystal structure by Xiao et al.[37] with the PDB code 3EGZ. Tetracycline is shown in green, and the three different spin label positions are shown in blue (C15), dark red (U18), and turquoise (C3). Mg^{2+} ions identified in the crystal structure are colored magenta as a ball presentation. The AAAA-motif in junction J1/2 is shown in purple. The expected crystal structure distances are 2.49 nm (TC-Mg^{2+}) and 2.17 nm (AAAA-Mg^{2+}) for C15, 3.13 and 3.62 nm for U18, and 3.15 and 1.79 nm for C3.

experiments performed in this study, the nitroxide spin was pumped and the Mn^{2+} spin was used for detection. An offset of $|\Delta\nu| = 80$ MHz was used, which corresponds to the detection of the Mn^{2+} electron spin transitions with larger electron spin states ($m_S > |\pm 1/2|$). Detecting the central Mn^{2+} electron spin state ($m_S = \pm 1/2$) yielded identical distance distributions (Figures S3 and S4). More experimental details can be found in the Supporting Information.

The first row of Figure 3 shows the PELDOR time domain data (left) and distance distributions (right) for TCAptC15. At 0.45 mM Mn^{2+} in the presence of TC (blue), two rather narrow peaks with mean distances of 2.2 and 2.4 nm are visible. These distances agree very well with the predicted distances from the crystal structure for AAAA-Mn^{2+} (2.17 nm) and TC-Mn^{2+} (2.49 nm). However, in the absence of TC (red), the distance peak attributed to TC-Mn^{2+} (2.4 nm) can no longer be identified. TC stabilizes the Mn^{2+} ion in the binding pocket with two direct oxygen coordinations.[37] A vanishing TC-Mn^{2+} distance peak in the absence of TC is therefore reasonable, as the Mn^{2+} in the binding pocket is expected to be much less stabilized. Less specific Mg^{2+} binding in the absence of TC was also suggested by fluorescence data fitted to a modified Hill equation. Depending on the position of the fluorescence-responsive 2-aminopurine nucleobase within the aptamer, different K_d values and Hill coefficients were obtained.[36] Not surprisingly, the distance peak at 2.4 nm is observed if a Mn^{2+} concentration of 0.22 mM Mn^{2+} is used, this time again in the presence of TC (green). Interestingly, the distance peak at 2.2 nm now has a probability that is smaller than that of the 2.2 nm distance peak at 0.45 mM Mn^{2+}. In fact, the decrease in probability of the 2.2 nm distance peak is very similar to the decrease in Mn^{2+} concentration (a decrease by a factor of 2). This suggests that at lower Mn^{2+} concentrations the divalent metal ion binding site belonging to the 2.2 nm distance peak is less occupied.

While the distance distribution data, based only on TCAptC15, suggest that the observed distance peak at 2.2 nm could belong to the divalent binding site at the AAAA-motif, the following concerns and circumstances should be considered. First, because the two distance peaks are very close to each other, they could be a regularization artifact. However, this is unlikely, as the bootstrapping confidence interval analysis of 1000 samples gives very narrow confidence intervals. Second, the distance peak at 2.2 nm and its near-perfect agreement with the expected distance for the AAAA-Mn^{2+} ion could be pure coincidence. Third, an almost identical distance distribution is obtained if the central Mn^{2+} electron spin state is detected (Figures S3 and S4, 0.45 mM Mn^{2+} w/ TC). This rules out the possibilities that the peak at 2.2 nm is caused by orientation selection or Mn^{2+} high spin contributions, with both contributions being expected to be small anyway.[43,44]

To investigate the origin of the 2.2 nm distance peak for TCAptC15 in detail, PELDOR experiments under the same experimental conditions were performed for TCAptU18 and TCAptC3. The results of TCAptU18 are shown in the middle row of Figure 3. At 0.45 mM Mn^{2+} and in the presence of TC (blue), two distinct distance peaks at 3.1 and 3.6 nm are visible. These distances again agree very well with the expected crystal structure distance of TCAptU18 for the TC-Mn^{2+} and AAAA-Mn^{2+} ions (Figure 2). As anticipated, the distance peak at 3.1 nm (TC-Mn^{2+}) is strongly attenuated if no TC is present (0.45 mM Mn^{2+} w/o TC, red), while the probability of the peak at 3.6 nm (AAAA-Mn^{2+}) remains unchanged. At lower Mn^{2+} concentrations of 0.22 mM, the peak at 3.1 nm is again observed. Now, the peak probability ratio $P_{\text{TC-Mn}^{2+}}(r)/P_{\text{AAAA-Mn}^{2+}}(r)$ is larger than that at 0.45 mM Mn^{2+}. The observation and conclusion of PELDOR data for TCAptU18 are therefore in perfect agreement with TCAptC15.

The bottom row of Figure 3 shows the PELDOR time domain data and distance distributions of TCAptC3. For 0.45 mM Mn^{2+} in the presence of TC (blue), two distinct distance peaks at 1.7 and 3.1 nm are visible. Again, these mean distances

https://doi.org/10.1021/acs.jpclett.3c02566
J. Phys. Chem. Lett. 2023, 14, 11421−11428

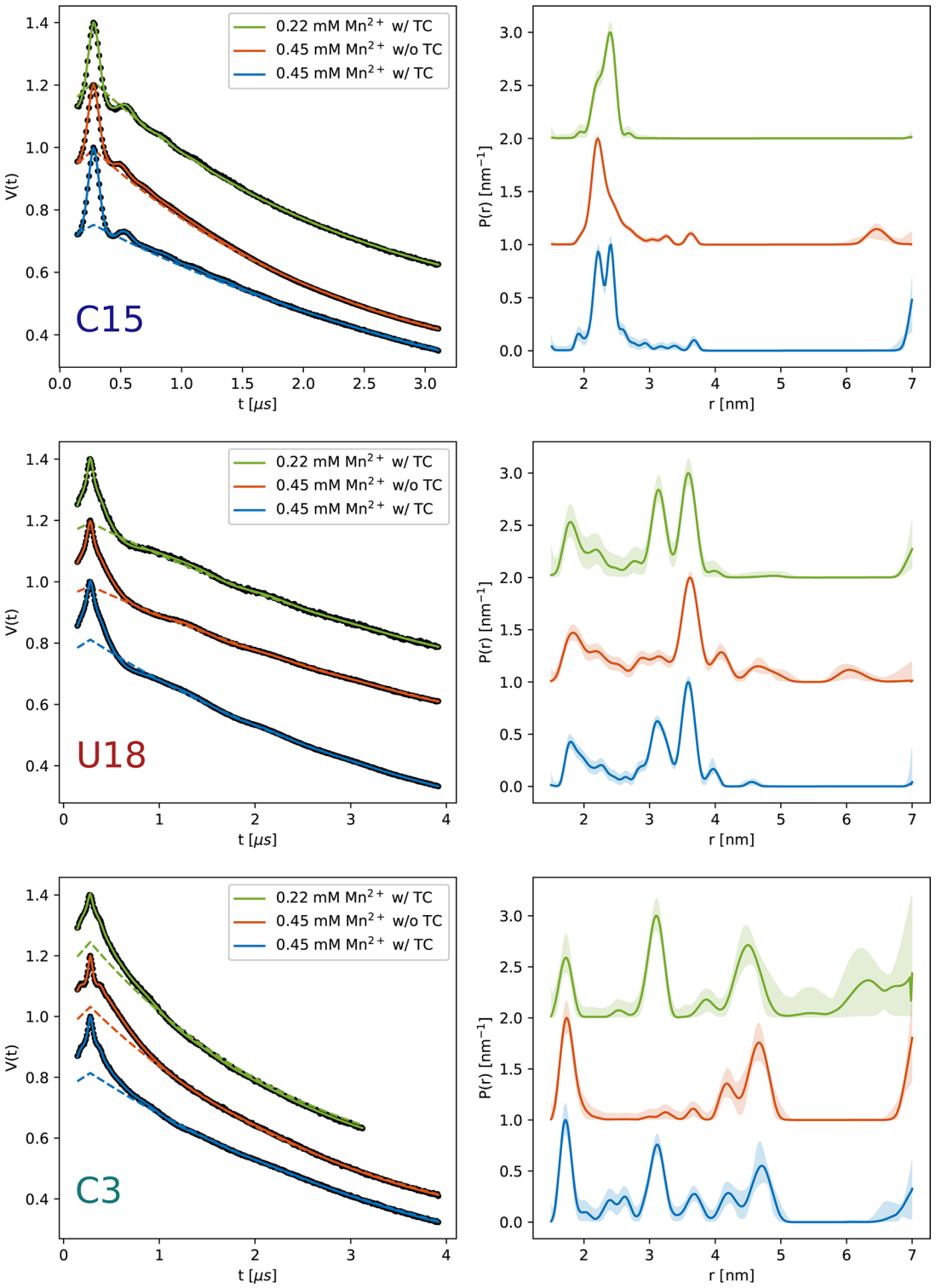

Figure 3. Nitroxide-Mn^{2+} PELDOR time domain data (left column) and the resulting distance distributions (right column) for different labeling positions. First row: TCAptC15; second row: TCAptU18; third row: TCAptC3. The primary PELDOR data are shown in black. Experiments were performed for different Mn^{2+} concentrations. Green: 0.22 mM Mn^{2+} in the presence of TC; red: 0.45 mM Mn^{2+} in the absence of TC; blue: 0.45 mM Mn^{2+} in the presence of TC. For the time domain data, the solid colorized lines correspond to the fits obtained with DeerLab.[42] The colorized dashed lines correspond to the unmodulated background function. For the distance domain data, the shaded areas correspond to the bootstrapped confidence intervals (95%, 1000 samples).

are in perfect agreement with the expected crystal structure distances for AAAA-Mn^{2+} (1.79 nm) and TC-Mn^{2+} (3.15 nm). The TC-Mn^{2+} distance peak disappears if no TC is present (0.45 mM Mn^{2+} w/TC, red). At a Mn^{2+} concentration of 0.22 mM in the presence of TC, the peak at 3.1 nm is again observed. The AAAA-Mn^{2+} peak at 1.7 nm now has a smaller probability than that at 0.45 mM, which is in perfect agreement with the AAAA-Mn^{2+} distance peak observations for

https://doi.org/10.1021/acs.jpclett.3c02566
J. Phys. Chem. Lett. 2023, 14, 11421−11428

Table 1. Comparison of Nitroxide-Mn^{2+} Distances for Different Labeling Positions[a]

	TC-Mn^{2+} (C15)/nm	AAAA-Mn^{2+} (C15)/nm	TC-Mn^{2+} (U18)/nm	AAAA-Mn^{2+} (U18)/nm	TC-Mn^{2+} (C3)/nm	AAAA-Mn^{2+} (C3)/nm
X-ray	2.49	2.17	3.13	3.62	3.15	1.79
PELDOR	2.41	2.21	3.12	3.59	3.11	1.72

[a]The distances were either extracted from a modified crystal structure or from PELDOR distance distributions.

TCAptC15 and TCAptU18. All distance distributions of TCAptC3 have a probability for very long distances (>6 nm), and these long distances are most likely artifacts from the background correction. All distance distributions from TCAptC3 also show rather undefined and broad distributions around 4.5 nm. The confidence intervals for the distances at 4.5 nm are smaller than for the distances > 6 nm but larger than the confidence intervals obtained for the TC-Mn^{2+} and AAAA-Mn^{2+} peaks.

Distance distributions of TCAptU18 and TCAptC3 each show a single distance peak with a considerable distance probability that cannot be easily explained. For TCAptU18 (Figure 3, middle row) this peak appears at around 1.9 nm, and for TCAptC3 (Figure 3, bottom row) the peak appears at 4.5 nm. These distances do not match with any of the expected distances for the other divalent metal ion binding sites that are present in the crystal structure (Table S2). The next closest divalent metal ion for the unassigned distance of TCAptU18 has already a difference of 0.65 nm (Mg 507); for TCAptC3 the difference for the next closest divalent metal ion is 0.32 nm (Mg 503). It is possible that the unassigned distance peaks could be caused by a divalent metal ion binding site that was not detected in the crystal structure. Figure 2 shows that TCAptC15 is somewhat located between TCAptC3 and TCAptU18. Therefore, the unassigned distance peaks of TCAptC3 and TCAptU18 indicate that such an unresolved metal binding site is very close to the spin label at position C15. In this case, the unresolved metal binding site cannot be detected with PELDOR or TCAptC15, as PELDOR cannot detect distances smaller than approximately 1.5 nm. With the labeling sites used in this study, this hypothesis cannot be conclusively clarified. It is known that crystal packing effects can alter the structure and orientation of RNAs observed under more physiological conditions.[45,46] It is highly unlikely that the unassigned distance peaks of TCAptC3 and TCAptU18 originate from additional rotamers of the spin labels. The difference of the unassigned distance peaks to the TC-Mn^{2+} distance peaks is >1 nm for both labeling sites, which is too large for an additional spin label rotamer. The spin label itself is only spanning 0.9 nm when measured from 2′-N to the oxygen atom of the NO bond.

Despite these two unassigned distance peaks, it was possible to observe the Mn^{2+} ion in the TC binding pocket with all three constructs, and all constructs showed an additional peak which could be assigned to the AAAA-Mn^{2+} ion. Other divalent metal ion binding sites of the TC aptamer (Table S2) are not an option for various reasons: (i) The assignment of the TC-Mn^{2+} ion is obvious, as this distance peak disappears for all three labeling sites. A strongly decreased affinity toward this Mn^{2+} ion is expected if TC, which forms two direct oxygen coordinations to the TC-Mn^{2+} ion, is not present. (ii) All three labeling sites were in perfect agreement with the crystal structure;[37] the difference of the extracted X-ray distance and the experimentally determined PELDOR distance was never more than 5%—this is true for both TC-Mn^{2+} and AAAA-Mn^{2+} (see Table 1). The only other metal ion resolved in the crystal structure that comes close to the AAAA-Mn^{2+} ion is divalent metal ion 502 (Table S2). However, for all three labeling sites, the experimental distances agree better with AAAA-Mn^{2+} than with metal ion 502. For labeling position C15, the difference of the experimental distance and the crystal structure distance of the AAAA-Mn^{2+} ion is negligible. The difference of the experimental distance assigned to the AAAA-Mn^{2+} ion and the crystal structure distance of metal ion 502 is already 0.25 nm. The low internal degree of freedom of the semirigid spin label is good enough to resolve such a difference. The difference to other divalent metal ions is even larger. For divalent metal ion 501, the difference is already >0.4 nm for all three labeling sites. (iii) The AAAA-Mn^{2+} ion is the only divalent metal ions besides the TC-Mn^{2+} ion that is directly coordinated by two oxygen atoms, thus suggesting a strong binding mode. Other metal ions have either no direct coordination or just one direct oxygen coordination (metal ion 502). With nitroxide-Mn^{2+} PELDOR, it was therefore possible to unambiguously locate and confirm an additional binding site with a high affinity.

The data presented in Figure 3 strongly suggest a smaller relative affinity of the AAAA-Mn^{2+} binding site in comparison to the TC-Mn^{2+} binding site. The smaller relative affinity of the AAAA-Mn^{2+} binding site becomes even clearer in Figure 4. Unlike those in Figure 3, the distance distributions for 0.22 mM (green) and 0.45 mM (blue) Mn^{2+} in the presence of TC for the three different constructs were normalized to the mean distance of the TC-Mn^{2+} peak.

In this presentation, it becomes clear that the probability of the AAAA-Mn^{2+} peak decreases for all three constructs if the Mn^{2+} concentration is decreased. This shows that the affinity of the AAAA-Mn^{2+} binding site is not as high as that of the TC-Mn^{2+} binding site, but it is still relatively high. An identical conclusion is obtained if Gaussian models are fitted to the nonparametric distance distributions, and the definite integral ratios of the TC-Mn^{2+} and AAAA-Mn^{2+} distance peaks are compared at different Mn^{2+} concentrations (Section 8 of the Supporting Information). Undoubtedly, the AAAA-Mn^{2+} binding site has the highest divalent metal ion affinity among all additional binding sites that were identified in the crystal structure. It should be added that two data points, i.e., at 0.22 and 0.45 mM Mn^{2+}, only allow for a qualitative interpretation of the affinity. For obtaining quantitative K_d values with PELDOR spectroscopy, more data points at different concentrations are needed.[47]

In Figure 4, the decrease in probability of the AAAA-Mn^{2+} peak is around 30% for constructs TCAptC15 and TCAptU18 and may not be clear upon a visual inspection of the primary PELDOR data. However, the confidence interval analysis shows that the decrease in probability is correct and not a regularization artifact. This highlights the ability of the PELDOR technique to directly localize divalent metal binding with high precision.

Quite often, the PDS of transition metals is hampered by complicated spin physics and a high flexibility of the spin label or the spin tag, which results in broad distance distributions.

https://doi.org/10.1021/acs.jpclett.3c02566
J. Phys. Chem. Lett. 2023, 14, 11421−11428

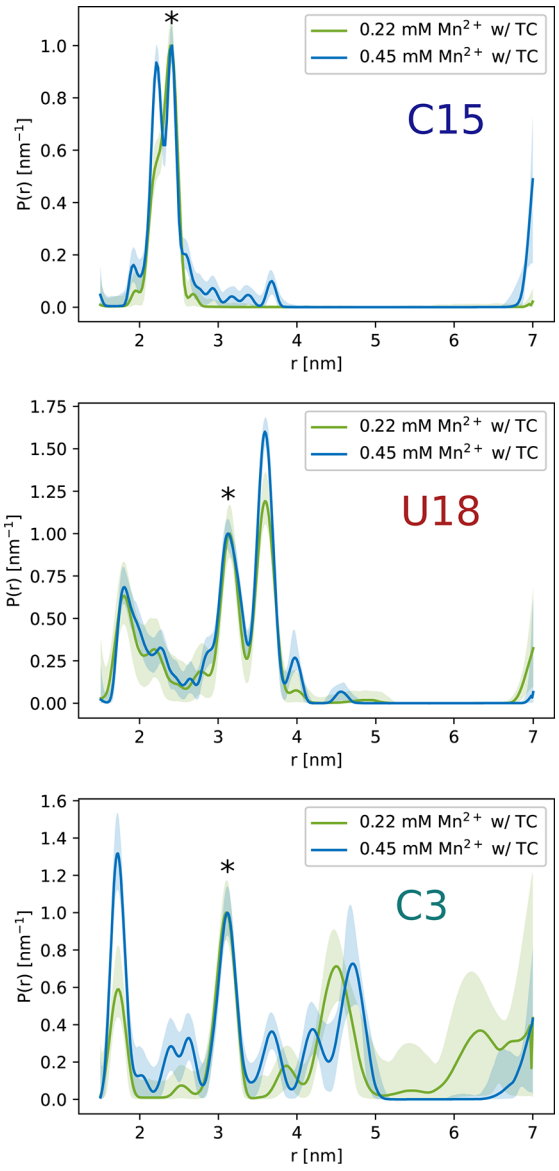

Figure 4. Comparison of distance distributions for different labeling sites in the presence of TC and with either 0.22 mM (green) or 0.45 mM (blue) Mn^{2+}. For the sake of clarity, the distance distributions were normalized to the probability of the TC-Mn^{2+} distance peak (marked with asterisks). First row: TCAptC15; second row: TCAptU18; third row: TCAptC3. The shaded areas correspond to the bootstrapped confidence intervals (95%, 1000 samples).

This makes it difficult to extract meaningful distance information. In this study, we present for the first time high quality nitroxide-Mn^{2+} PELDOR data of nucleic acids that localize two divalent metal-ion binding sites. It was possible to localize both the Mn^{2+} ion in the TC binding pocket and the one located at the AAAA-motif in the J1/2 junction. Both metal ion binding sites were present in the crystal structure by Xiao et al. along with several other additional divalent metal ions. The high affinity of the binding site at the AAAA-motif is not unexpected and can be explained by the rather unusual U-shaped turn of the phosphate backbone in this region.[37] The positively charged Mn^{2+} ion is required to compensate for the negative charges of the backbone, which are in proximity due to the U-shaped turn. PELDOR is one of the few spectroscopy techniques that can directly probe and monitor paramagnetic transition metals. It is complementary to X-ray crystallography, which can give a highly resolved three-dimensional framework in the sense that PELDOR is used to investigate more dynamic processes. In this study, the difference between the extracted crystal structure distances and experimentally determined PELDOR distances never exceeded 5%. We have shown here that a combination of a semirigid nitroxide spin label and PELDOR spectroscopy simultaneously localized two Mg^{2+} binding sites within the tetracycline RNA aptamer and revealed the relative binding affinity of these sites. Thus, the PELDOR technique, which can be applied to samples in frozen solutions and does not require highly diffracting crystals, can localize divalent metal ions that may play an essential role in the function of nucleic acids.

■ ASSOCIATED CONTENT

Supporting Information

The Supporting Information is available free of charge at https://pubs.acs.org/doi/10.1021/acs.jpclett.3c02566.

Additional information on the synthesis and purification of the RNA, experimental parameters used for the PELDOR measurements, and more experimental PELDOR results (PDF)

■ AUTHOR INFORMATION

Corresponding Author

Thomas F. Prisner − *Institute of Physical and Theoretical Chemistry and Center of Biomolecular Magnetic Resonance, Goethe University Frankfurt, 60438 Frankfurt am Main, Germany;* orcid.org/0000-0003-2850-9573; Email: Prisner@Chemie.Uni-Frankfurt.de

Authors

Thilo Hetzke − *Institute of Physical and Theoretical Chemistry and Center of Biomolecular Magnetic Resonance, Goethe University Frankfurt, 60438 Frankfurt am Main, Germany*

Marc Vogel − *Department of Biology, Technical University of Darmstadt, 64287 Darmstadt, Germany*

Anna-Lena Johanna Halbritter − *Department of Chemistry, Science Institute, University of Iceland, 107 Reykjavik, Iceland*

Subham Saha − *Department of Chemistry, Science Institute, University of Iceland, 107 Reykjavik, Iceland*

Beatrix Suess − *Department of Biology, Technical University of Darmstadt, 64287 Darmstadt, Germany;* orcid.org/0000-0001-8666-6716

Snorri Th. Sigurdsson − *Department of Chemistry, Science Institute, University of Iceland, 107 Reykjavik, Iceland;* orcid.org/0000-0003-2492-1456

Complete contact information is available at: https://pubs.acs.org/10.1021/acs.jpclett.3c02566

Notes

The authors declare no competing financial interest.

■ ACKNOWLEDGMENTS

Parts of some figures were created with the open-source molecular visualization software PyMOL. T.F.P, S.Th.S., and B.S. acknowledge financial support from the Collaborative Research Center 902 - Molecular Principles of RNA-based regulation of the German Research Foundation (3214020004).

S.Th.S. acknowledges financial support from the Icelandic Research Fund (206708).

REFERENCES

(1) Draper, D. E. A Guide to Ions and RNA Structure. *RNA* **2004**, *10*, 335−343.

(2) Lipfert, J.; Doniach, S.; Das, R.; Herschlag, D. Understanding Nucleic Acid-Ion Interactions. *Annu. Rev. Biochem.* **2014**, *83*, 813−841.

(3) Maderia, M.; Hunsicker, L. M.; DeRose, V. J. Metal-Phosphate Interactions in the Hammerhead Ribozyme Observed by ^{31}P NMR and Phosphorothioate Substitutions. *Biochemistry* **2000**, *39*, 12113−12120.

(4) Kim, H. D.; Nienhaus, G. U.; Ha, T.; Orr, J. W.; Williamson, J. R.; Chu, S. Mg^{2+}-Dependent Conformational Change of RNA Studied by Fluorescence Correlation and FRET on Immobilized Single Molecules. *Proc. Natl. Acad. Sci. U. S. A.* **2002**, *99*, 4284−4289.

(5) Qiu, X.; Andresen, K.; Kwok, L. W.; Lamb, J. S.; Park, H. Y.; Pollack, L. Inter-DNA Attraction Mediated by Divalent Counterions. *Phys. Rev. Lett.* **2007**, *99*, No. 038104.

(6) Zheng, H.; Shabalin, I. G.; Handing, K. B.; Bujnicki, J. M.; Minor, W. Magnesium-Binding Architectures in RNA Crystal Structures: Validation, Binding Preferences, Classification and Motif Detection. *Nucleic Acids Res.* **2015**, *43*, 3789−3801.

(7) Cunha, R. A.; Bussi, G. Unraveling Mg^{2+}-RNA Binding with Atomistic Molecular Dynamics. *RNA* **2017**, *23*, 628−638.

(8) Fuertig, B.; Richter, C.; Woehnert, J.; Schwalbe, H. NMR Spectroscopy of RNA. *ChemBioChem* **2003**, *4*, 936−962.

(9) Zhou, Y.; Chen, S.-J. Graph Deep Learning Locates Magnesium Ions in RNA. *QRB Discovery* **2022**, *3*, No. e20.

(10) Hubbell, W. L.; Gross, A.; Langen, R.; Lietzow, M. A. Recent Advances in Site-Directed Spin Labeling of Proteins. *Curr. Opin. Struct. Biol.* **1998**, *8*, 649−656.

(11) Qin, P. Z.; Hideg, K.; Feigon, J.; Hubbell, W. L. Monitoring RNA Base Structure and Dynamics Using Site-Directed Spin Labeling. *Biochemistry* **2003**, *42*, 6772−6783.

(12) Höbartner, C.; Sicoli, G.; Wachowius, F.; Gophane, D. B.; Sigurdsson, S. T. Synthesis and Characterization of RNA Containing a Rigid and Nonperturbing Cytidine-Derived Spin Label. *J. Org. Chem.* **2012**, *77*, 7749−7754.

(13) Cekan, P.; Smith, A. L.; Barhate, N.; Robinson, B. H.; Sigurdsson, S. T. Rigid Spin-Labeled Nucleoside Ç: A Nonperturbing EPR Probe of Nucleic Acid Conformation. *Nucleic Acids Res.* **2008**, *36*, 5946−5954.

(14) Piton, N.; Schiemann, O.; Mu, Y.; Stock, G.; Prisner, T.; Engels, J. W. Synthesis of Spin-Labeled RNAs for Long Range Distance Measurements by PELDOR. *Nucleos. Nucleot. Nucl.* **2005**, *24*, 771−775.

(15) Saha, S.; Jagtap, A. P.; Sigurdsson, S. T. Site-Directed Spin Labeling of 2'-Amino Groups in RNA with Isoindoline Nitroxides That Are Resistant to Reduction. *Chem. Commun.* **2015**, *51*, 13142−13145.

(16) Kerzhner, M.; Matsuoka, H.; Wuebben, C.; Famulok, M.; Schiemann, O. High-Yield Spin Labeling of Long RNAs for Electron Paramagnetic Resonance Spectroscopy. *Biochemistry* **2018**, *57*, 2923−2931.

(17) Asada, M.; Mino, H. Location of the High-Affinity Mn^{2+} Site in Photosystem II Detected by PELDOR. *J. Phys. Chem. B* **2015**, *119*, 10139−10144.

(18) Abdullin, D.; Schiemann, O. Pulsed Dipolar EPR Spectroscopy and Metal Ions: Methodology and Biological Applications. *ChemPlusChem.* **2020**, *85*, 353−372.

(19) Kaminker, I.; Bye, M.; Mendelman, N.; Gislason, K.; Sigurdsson, S. T.; Goldfarb, D. Distance Measurements between Manganese(II) and Nitroxide Spin-Labels by DEER Determine a Binding Site of Mn^{2+} in the HP92 Loop of Ribosomal RNA. *Phys. Chem. Chem. Phys.* **2015**, *17*, 15098−15102.

(20) Kisseleva, N.; Khvorova, A.; Westhof, E.; Schiemann, O. Binding of Manganese(II) to a Tertiary Stabilized Hammerhead Ribozyme as Studied by Electron Paramagnetic Resonance Spectroscopy. *RNA* **2005**, *11*, 1−6.

(21) Rudolph, M.; Tampé, R.; Joseph, B. Time-Resolved Mn2+-NO and NO-NO Distance Measurements Reveal That Catalytic Asymmetry Regulates Alternating Access in an ABC Transporter. *Angew. Chemie Int. Ed.* **2023**, *62* (37), No. e202307091.

(22) Pannier, M.; Veit, S.; Godt, A.; Jeschke, G.; Spiess, H. Dead-Time Free Measurement of Dipole-Dipole Interactions between Electron Spins. *J. Magn. Reson.* **2000**, *142*, 331−340.

(23) Martin, R. E.; Pannier, M.; Diederich, F.; Gramlich, V.; Hubrich, M.; Spiess, H. W. Determination of End-to-End Distances in a Series of TEMPO Diradicals of up to 2.8 Nm Length with a New Four-Pulse Double Electron Electron Resonance Experiment. *Angew. Chemie Int. Ed.* **1998**, *37*, 2833−2837.

(24) Berens, C.; Thain, A.; Schroeder, R. A Tetracycline-Binding RNA Aptamer. *Bioorg. Med. Chem.* **2001**, *9*, 2549−2556.

(25) Muller, M.; Weigand, J. E.; Weichenrieder, O.; Suess, B. Thermodynamic Characterization of an Engineered Tetracycline-Binding Riboswitch. *Nucleic Acids Res.* **2006**, *34*, 2607−2617.

(26) Weigand, J. E.; Suess, B. Tetracycline Aptamer-Controlled Regulation of Pre-MRNA Splicing in Yeast. *Nucleic Acids Res.* **2007**, *35*, 4179−4185.

(27) Kötter, P.; Weigand, J. E.; Meyer, B.; Entian, K.-D.; Suess, B. A Fast and Efficient Translational Control System for Conditional Expression of Yeast Genes. *Nucleic Acids Res.* **2009**, *37*, No. e120.

(28) Vogel, M.; Weigand, J. E.; Kluge, B.; Grez, M.; Suess, B. A Small, Portable RNA Device for the Control of Exon Skipping in Mammalian Cells. *Nucleic Acids Res.* **2018**, *46*, No. e48.

(29) Hanson, S.; Berthelot, K.; Fink, B.; McCarthy, J. E. G.; Suess, B. Tetracycline-Aptamer-Mediated Translational Regulation in Yeast. *Mol. Microbiol.* **2003**, *49* (6), 1627−1637.

(30) Hanson, S.; Bauer, G.; Fink, B.; Suess, B. Molecular Analysis of a Synthetic Tetracycline-Binding Riboswitch. *RNA* **2005**, *11*, 503−511.

(31) Hetzke, T.; Vogel, M.; Gophane, D. B.; Weigand, J. E.; Suess, B.; Sigurdsson, S. T.; Prisner, T. F. Influence of Mg^{2+} on the Conformational Flexibility of a Tetracycline Aptamer. *RNA* **2019**, *25*, 158−167.

(32) Hetzke, T.; Bowen, A. M.; Vogel, M.; Gauger, M.; Suess, B.; Prisner, T. F. Binding of Tetracycline to Its Aptamer Determined by 2D-Correlated Mn^{2+} Hyperfine Spectroscopy. *J. Magn. Reson.* **2019**, *303*, 105−114.

(33) Förster, U.; Weigand, J. E.; Trojanowski, P.; Suess, B.; Wachtveitl, J. Conformational Dynamics of the Tetracycline-Binding Aptamer. *Nucleic Acids Res.* **2012**, *40*, 1807−1817.

(34) Wunnicke, D.; Strohbach, D.; Weigand, J. E.; Appel, B.; Feresin, E.; Suess, B.; Muller, S.; Steinhoff, H.-J. Ligand-Induced Conformational Capture of a Synthetic Tetracycline Riboswitch Revealed by Pulse EPR. *RNA* **2011**, *17*, 182−188.

(35) Reuss, A. J.; Vogel, M.; Weigand, J. E.; Suess, B.; Wachtveitl, J. Tetracycline Determines the Conformation of Its Aptamer at Physiological Magnesium Concentrations. *Biophys. J.* **2014**, *107*, 2962−2971.

(36) Kaiser, C.; Vogel, M.; Appel, B.; Weigand, J.; Müller, S.; Suess, B.; Wachtveitl, J. Magnesium Ion-Driven Folding and Conformational Switching Kinetics of Tetracycline Binding Aptamer: Implications for in Vivo Riboswitch Engineering. *J. Mol. Biol.* **2023**, *435* (20), No. 168253.

(37) Xiao, H.; Edwards, T. E.; Ferré-D'Amaré, A. R. Structural Basis for Specific, High-Affinity Tetracycline Binding by an in Vitro Evolved Aptamer and Artificial Riboswitch. *Chem. Biol.* **2008**, *15*, 1125−1137.

(38) Abdullin, D.; Florin, N.; Hagelueken, G.; Schiemann, O. EPR-Based Approach for the Localization of Paramagnetic Metal Ions in Biomolecules. *Angew. Chemie Int. Ed.* **2015**, *54*, 1827−1831.

(39) Saha, S.; Hetzke, T.; Prisner, T. F.; Sigurdsson, S. T. Noncovalent Spin-Labeling of RNA: The Aptamer Approach. *Chem. Commun.* **2018**, *54*, 11749−11752.

(40) Erlenbach, N.; Grünewald, C.; Krstic, B.; Heckel, A.; Prisner, T. F. End-to-End Stacking of Small DsRNA. *RNA* **2019**, *25*, 239−246.

https://doi.org/10.1021/acs.jpclett.3c02566
J. Phys. Chem. Lett. 2023, 14, 11421−11428

(41) Jeschke, G. DEER Distance Measurements on Proteins. *Annu. Rev. Phys. Chem.* **2012**, *63*, 419−446.
(42) Fábregas Ibáñez, L.; Jeschke, G.; Stoll, S. DeerLab: A Comprehensive Software Package for Analyzing Dipolar Electron Paramagnetic Resonance Spectroscopy Data. *Magn. Reson.* **2020**, *1*, 209−224.
(43) Vincent Ching, H. Y.; Demay-Drouhard, P.; Bertrand, H. C.; Policar, C.; Tabares, L. C.; Un, S. Nanometric Distance Measurements between Mn^{2+}-DOTA Centers. *Phys. Chem. Chem. Phys.* **2015**, *17*, 23368−23377.
(44) Dalaloyan, A.; Qi, M.; Ruthstein, S.; Vega, S.; Godt, A.; Feintuch, A.; Goldfarb, D. Gd(III)-Gd(III) EPR Distance Measurements - the Range of Accessible Distances and the Impact of Zero Field Splitting. *Phys. Chem. Chem. Phys.* **2015**, *17*, 18464−18476.
(45) Sickmier, E. A.; Frato, K. E.; Shen, H.; Paranawithana, S. R.; Green, M. R.; Kielkopf, C. L. Structural Basis for Polypyrimidine Tract Recognition by the Essential Pre-MRNA Splicing Factor U2AF65. *Mol. Cell* **2006**, *23*, 49−59.
(46) Simon, B.; Madl, T.; Mackereth, C. D.; Nilges, M.; Sattler, M. An Efficient Protocol for NMR-Spectroscopy-Based Structure Determination of Protein Complexes in Solution. *Angew. Chemie Int. Ed.* **2010**, *49*, 1967−1970.
(47) Glaenzer, J.; Peter, M. F.; Thomas, G. H.; Hagelueken, G. PELDOR Spectroscopy Reveals Two Defined States of a Sialic Acid TRAP Transporter SBP in Solution. *Biophys. J.* **2017**, *112*, 109−120.

https://doi.org/10.1021/acs.jpclett.3c02566
J. Phys. Chem. Lett. 2023, 14, 11421−11428